

Docking studies of a Triazole-based Chalcone on Various Matrix Metalloproteinases

Omar A. Soliman ^{1, 2, #}, Kholoud K. Debes ^{3, #}, Nesreen S. Haiba ⁴, Reda M. Keshk ³, Doha M. Beltagy ⁵, Mohamed Teleb ^{6, *}, Abdel Moneim El Massry ⁷, Sherine N. Khattab ^{7, *}

¹ Department of Clinical Pharmacy, Alexandria University Main Teaching Hospital, Alexandria, Egypt.

² Department of Human Genetics, Medical Research Institute, Alexandria University, Alexandria, Egypt.

³ Chemistry Department, Faculty of Science, Damanhour University, Damanhour 22511, Egypt.

⁴ Department of Physics and Chemistry, Faculty of Education, Alexandria University, Egypt.

⁵ Biochemistry Department, Faculty of Science, Damanhour University, Damanhour 22511, Egypt.

⁶ Department of Pharmaceutical Chemistry, Faculty of Pharmacy, Alexandria University, Alexandria 21521, Egypt.

⁷ Chemistry Department, Faculty of Science, Alexandria University, Alexandria 21321, Egypt.

* Correspondence Address:

Sherine N. Khattab: Chemistry Department, Faculty of Science, Alexandria University, Alexandria 21321, Egypt. Email address: sherinekhattab@alexu.edu.eg; sh.n.khattab@gmail.com.

Mohamed Teleb: Department of Pharmaceutical Chemistry, Faculty of Pharmacy, Alexandria University, Alexandria 21521, Egypt. Email address: mohamed.t.ismail@alexu.edu.eg.

Omar A. Soliman and Kholoud K. Debes have equal contribution.

KEYWORDS: Molecular Modelling; Docking; MMPs; Cancer; Triazole; Chalcone

Received:

December 25, 2024

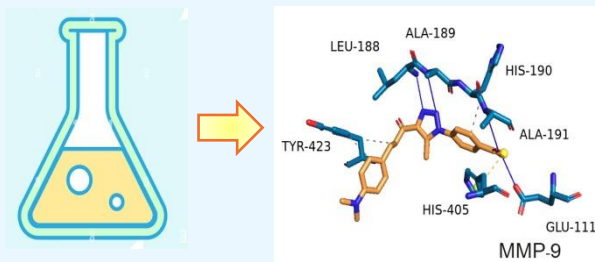
Accepted:

January 03, 2025

Published:

January 17, 2025

ABSTRACT: Docking is a powerful tool that has been validated for lead optimization. Cancer research has been always concerned with matrix metalloproteinases (MMPs) inhibition being a validated druggable target that is implicated in almost all stages of carcinogenesis. Therefore, optimization of lead inhibitors is of utmost importance. The present study explores the possible binding modes of a novel triazole-based chalcone into various MMPs catalytic domains in attempt to explore its potential as possible MMP inhibitors, identify its isoform selectivity and deduce the structural determinants of activity within the scaffold. The investigated chalcone, referred to as compound **3**, demonstrated preferential binding to MMP-9 and MMP-13 in terms of favorable binding energies (-11.92 and -11.25 kcal/mol), inhibition constants (1.82 and 5.65 nM), electrostatic (-0.38 and -0.14 Kcal/mol) and vdW (-13.63 and -13.32 Kcal/mol, respectively) interactions referring to its potential utility for targeted selective tumor associated MMPs inhibition. These results encourage further research to evaluate the compound's *in vitro* potency of the studied compound against MMP-9 and MMP-13 and sensitive cancer cell lines.



1. INTRODUCTION

Cancer research focuses on tumor microenvironment modulation, especially the extracellular matrix, that promotes proliferation of tumor cells and metastasis [1,2]. Various

proteinases are released into the extracellular matrix to influence tumor progression [3]. Matrix metalloproteinases (MMPs), a family of zinc-dependent endopeptidases, are among the most

vital ones that are dysregulated in nearly all human cancers [4-6]. To date, about 26 MMPs have been well identified and classified into collagenases (MMP-1, -8, -13, -18), gelatinases (MMP-2, -9), stromelysins (MMP-3, -10), matrilysins (MMP-7, -26), membrane-type MMPs (MMP-14 to -25), and others [7]. All these isoforms share a structurally similar catalytic domain, comprising an active site zinc ion coordinated by three histidine residues. The domain is divided into N-terminal and C-terminal subdomains by a shallow cleft containing six binding pockets (S1, S2, S3, S1', S2', and S3'), with the S1' subsite serving as the selectivity pocket among various MMPs [8,9]. MMPs have emerged over the last three decades as attractive anticancer targets. Active medicinal chemistry research introduced numerous MMP inhibitors [10-13]. Initial MMP inhibitors were designed as peptidomimetic mimics of endogenous MMPs ligands incorporating a hydroxamic acid group to bind the active site zinc. Despite their unmet potency, these inhibitors failed clinically due to side effects [10], dose-limiting toxicity [14], and pharmacokinetic challenges [15] associated with the hydroxamic acid moiety [16,17]. These limitations prompted efforts to diversify the zinc-binding groups, resulting in the development of non-hydroxamate MMPs inhibitors in a trial to avoid off target side effects [18,19]. Further research has focused on designing selective inhibitors for individual MMPs. Indeed, designing inhibitors that spare the hydroxamic acid group while maintaining potency remains a significant challenge. Generally, these non-hydroxamates tend to be molecules with linked planar rings with amino and carbonyl moieties that facilitate hydrophilic interactions with the active site. These structural features may be viewed thematic among the class [20-22]. In our recent studies, we have optimized new series of non-hydroxamate MMP-2, -9, -10 and -13 inhibitors and identified potent lead compounds [23-30] (Figure 1). Some inhibitors based on triazole-tethered chalcones surpassed the well-known reference broad-spectrum hydroxamate-based MMPs inhibitor *N*-hydroxy-2-[(4-methoxyphenyl)sulfonylamino]-acetamide (NNGH) with considerable isoform selectivity [31]. Interestingly, these lead compounds were capable of halting non-small cell lung cancer (NSCLC) [30], colorectal and liver cancers [29].

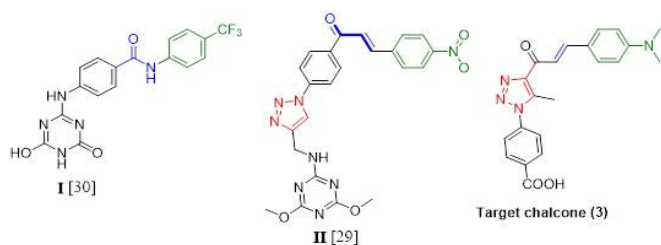


Figure 1. Lead MMPs inhibitors (I-II)^{29,30} and the designed chalcone derivative (3).

2. Design rationale

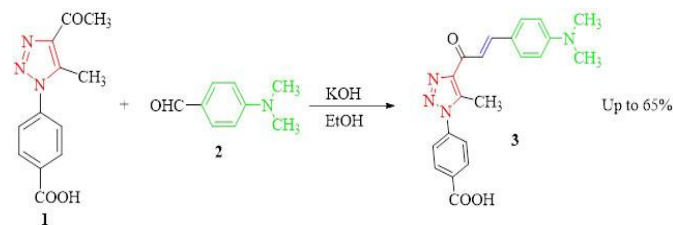
Building on these findings together with the literature referring to the anticancer potential of chalcones especially those tethered to azoles [32], we present a computational investigation of the binding modes of a newly designed chalcone-tethered triazole-carboxylic acid derivative (I) within various MMPs active sites. The study aims to gain preliminary insights into the possible

structural determinants underlying the activity of this compound for guiding further derivatization and subsequent biological studies. It is worth mentioning that docking simulations play a pivotal role in ligand optimization process [26] and identification of potential inhibitors from natural sources [33-36]. At a qualitative level, this approach helps identifying the key interactions between ligands and their binding pockets, predicting ligands-induced rearrangements within the pockets, and refining potential ligand poses [37,38]. Techniques such as Molecular Mechanics/Poisson-Boltzmann Surface Area (MM/PBSA) deliver precise binding energy estimates [39].

3. Results and discussion

3.1. Chemistry

The desired chalcone was prepared by adding 4-(4-acetyl-5-methyl-1*H*-1,2,3-triazol-1-yl)benzoic acid **1** to potassium hydroxide dissolved in a small amount of water, then 20 mL ethanol was added. The previous mixture was allowed to stir for about 10 minutes at room temperature. 4-(Dimethylamino)benzaldehyde **2** was further added then the reaction mixture was allowed to stir for about 72 h at room temperature. Excess amount of KOH dissolved in a minimal amount of water may added during the reaction period until the reaction was completed the reaction mixture was kept in an ice bath while adding KOH to prevent overheating. Once the reaction was completed, the reaction mixture was neutralized using iced 1 N HCl until complete precipitation. The resulting solid was filtered off, washed well with cold water and recrystallized from methanol afforded the pure product **3** (Scheme 1).



Scheme 1. Synthesis of (*E*)-4-(4-(3-(4-(dimethylamino)phenyl)acryloyl)-5-methyl-1*H*-1,2,3-triazol-1-yl)benzoic acid **3**.

The desired chalcone **3** was obtained as orange powder, 0.4 g (65%) yield; Melting: 248-250°C. Structure of the prepared compound was confirmed by different spectroscopic techniques such as IR, ¹H NMR, ¹³C-NMR and elemental analysis. The IR spectra of (*E*)-4-(4-(3-(4-(dimethylamino)phenyl)acryloyl)-5-methyl-1*H*-1,2,3-triazol-1-yl)benzoic acid **3** showed a broad, strong absorption band between 3439 and 2556 cm⁻¹, corresponding to the OH stretching of carboxylic acid. Additionally, the carbonyl stretching vibrations (C=O) for carboxylic acid and chalcone were detected at 1720 cm⁻¹ and 1604 cm⁻¹, respectively. The carbonyl signal of the carboxylic acid appears at a higher wavenumber than that of the chalcone, which can be attributed to the electronegativity associated with the OH group and the resonance effect.

The ¹H-NMR spectrum of compound **3** in DMSO-*d*₆ showed two singlet peaks at the aliphatic region. Singlet peak observed at chemical shift of 2.60 ppm. correspond to the C⁵-triazole methyl group protons. Another singlet peak equivalent to six

protons was also observed at chemical shift 2.97 ppm corresponding to the two methyl groups of the aldehyde moiety. Aromatic protons were observed as four peaks three doublets and one multiplet peak. First doublet peak was observed at chemical shift 6.71 ppm corresponding to two aromatic protons with $J = 9$ Hz. Second peak observed at δ 7.60 ppm also corresponding to two aromatic protons with $J = 8.95$ Hz. The last aromatic doublet peak was observed at δ 8.14 ppm with $J = 8.5$ Hz. The remaining aromatic protons were combined with the chalcone protons ($\text{CH}=\text{CH}-\text{CO}$) and presented as multiplet peak within the chemical shift range 7.69-7.80 ppm. Finally, proton of the carboxylic group appeared as broad singlet peak at chemical shift 13.39 ppm

The ^{13}C -NMR spectrum of the compound **3** in $\text{DMSO}-d_6$ showed 15 resolved carbon signals, Three peaks in the aliphatic region appeared 10.53, 39.50 and 40.50 ppm corresponding to the three methyl groups. There are 12 peaks at the aromatic region for (SP^2 Ar-C, SP^2 $\text{CH}=\text{CH}-\text{CO}$) at chemical shifts 112.41, 117.31, 122.12, 125.98, 131.22, 132.58, 138.94, 144.10, 144.82 and 152.65 ppm. The final two peaks, appeared at 166.94 and 183.52 ppm, correspond to the two carbonyl carbons in (COOH , $\text{CH}=\text{CH}-\text{CO}$), respectively. The carbonyl carbon in the chalcone structure is more stable than that of the carboxylic acid due to the resonance effect. Overall, the chalcone ($\text{CH}=\text{CH}-\text{CO}$) is more deshielded compared to its neighboring carbon atoms.

3.2. Docking studies

This study employs computational docking simulations to investigate the binding interactions of compound **3** with various matrix metalloproteinases (MMPs), including MMP-2, MMP-8, MMP-9, MMP-10, and MMP-13. Molecular docking techniques provide an efficient approach for predicting binding poses, binding affinities, and the structural determinants influencing ligand-protein interactions. The binding site residues were mapped, providing critical information for setting up the docking grid. These coordinates were later used to define the docking box and the center of the grid for molecular docking simulations. A grid parameter file (GPF) was prepared to specify the docking region on the protein. The grid was centered at coordinates drawn from the PLIP analysis shown in Table 1.

Table 1: Metalloproteinases with their respective associated PDB code and the XYZ coordinates used for producing GPF file pre-docking production.

PDB Code	Protein Associated	X-Coordinate	Y-Coordinate	Z-Coordinate
2OW9 [40]	MMP-13	52.066	10.13	9.8583
1Q3A [41]	MMP-10	24.440	-6.957	23.012
1GKC [42]	MMP-9	61.909	28.983	114.582
5H8X [43]	MMP-8	-8.244	-12.355	20.882
8H78 [44]	MMP-2	27.634	22.189	-6.661

The docking results, summarized in Tables 2-6, reveal critical

insights into the molecular interactions, such as van der Waals (vdW) forces, electrostatic interactions, and inhibition constants, offering a quantitative basis for understanding the ligand's inhibitory potential.

The computational docking investigations revealed substantial binding interactions between compound **3** and the five evaluated MMP proteins (Table 7). MMP-9 demonstrated the most pronounced binding affinity, exhibiting a remarkable binding energy of -11.92 kcal/mol, with MMP-13 following closely at -11.25 kcal/mol. These computational findings indicate the formation of energetically stable and robust molecular complexes between compound **3** and the target MMPs. The inhibition constants (K_i) corroborated the strong binding affinity, particularly for MMP-9 (1.82 nM) and MMP13 (5.65 nM), indicative of high inhibitory potential. For MMP-2, a moderate inhibition constant of 22.02 nM was observed, while MMP-8 (54.99 nM) and MMP-10 (572.68 nM) showed relatively weaker inhibition. This suggests that compound **3** preferentially inhibits MMP-9 and MMP-13 over the other MMPs.

Analysis of the docking poses revealed that van der Waals (vdW) interactions and electrostatic forces were key contributors to the stability of the compound **3**-MMP complexes; for MMP-9 and MMP-13, strong vdW interactions were observed, supporting their superior binding energies. Electrostatic interactions, particularly hydrogen bonds and metal ion coordination, further stabilised these complexes. In contrast, MMP-10 displayed weaker electrostatic contributions, reflected in its relatively high inhibition constant and lower binding energy (-8.52 kcal/mol). Similarly, MMP-8 exhibited moderate vdW and electrostatic interactions, resulting in an intermediate binding profile. Moreover, Ligand efficiency (LE) scores were highest for MMP-9 (-0.43) and MMP-13 (-0.40), underscoring the efficient use of compound **3** molecular structure to achieve favourable binding. Lower LE scores for MMP-8 and MMP-10 indicate less efficient binding, potentially due to suboptimal interactions within the active sites. The most stable docking interactions are illustrated in Figures 2-6. Regarding MMP-2, compound **3** formed strong hydrophobic interactions and hydrogen bonds with key active-site residues, including ASP77, GLU103, and LEU82. Metal ion coordination with calcium at the active site further stabilised the interaction. The electrostatic environment contributed to its moderate inhibition constant of 22.02 nM. The interaction profile of MMP-8 revealed that compound **3** engaged key residues such as ASP137, GLY169, and HIS162 through hydrophobic and hydrogen bonding interactions. Ionic interactions with the active-site residues complemented the binding but were less significant in enhancing the inhibition constant (54.99 nM). Compound **3**'s most substantial interaction with MMP-9 involved residues such as ASP182, GLY183, and TYR187, forming extensive hydrophobic contacts and hydrogen bonds. Metal coordination with calcium ions in the active site was crucial in stabilising the complex, resulting in the lowest inhibition constant of 1.82 nM. Interactions with residues such as ASP174, GLY175, and HIS217 characterised the binding of compound **3** to MMP-10. The hydrophobic and electrostatic interactions were weaker than other MMPs, reflected in the high inhibition constant of 572.68 nM. Finally, compound **3** displayed robust interactions toward MMP-13 with ASP158, GLY159, and TYR223. The active site

facilitated strong hydrophobic contacts, significant hydrogen bonding, and metal ion coordination. These interactions resulted

in a low inhibition constant of 5.65 nM, highlighting compound **3** effectiveness as an MMP-13 inhibitor.

Table 2. Docking results of chalcone derivative **3** into the MMP-13 (PDB: 2OW9) catalytic domain. Binding, Intermolecular, VdW, and Electrostatic Energy are reported in kcal/mol; Ligand Efficiency is in kcal/mol/atom; and the Inhibition Constant is in nM.

Pose	Binding Energy (Kcal/mol)	Ligand Efficiency (Kcal/mol/atom)	Inhibition Constant (nM)	Intermolecular Energy (Kcal/mol)	Vdw Energy (Kcal/mol)	Electrostatic Energy (Kcal/mol)
1	-11.25	-0.4	5.65	-13.34	-13.32	-0.14
2	-10.21	-0.36	32.82	-12.32	-12.33	-0.03
3	-10.18	-0.36	34.33	-12.27	-11.82	-0.45
4	-10.02	-0.36	45.02	-12.11	-11.72	-0.39
5	-9.62	-0.34	88.53	-11.71	-11.54	-0.17
6	-6.67	-0.24	12.92	-8.76	-8.62	-0.14
7	-6.20	-0.22	28.31	-8.29	-8.23	-0.07
8	-5.61	-0.2	77.3	-7.7	-7.54	-0.16
9	-4.38	-0.16	619.4	-6.46	-6.50	-0.03

Table 3. Docking results of chalcone derivative **3** into MMP-10 (PDB: 1Q3A) catalytic domain. Binding, Intermolecular, VdW, and Electrostatic Energy are reported in kcal/mol; Ligand Efficiency is in kcal/mol/atom; and the Inhibition Constant is in nM catalytic domain.

Pose	Binding Energy (Kcal/mol)	Ligand Efficiency (Kcal/mol/atom)	Inhibition Constant (nM)	Intermolecular Energy (Kcal/mol)	Vdw Energy (Kcal/mol)	Electrostatic Energy (Kcal/mol)
1	-8.52	-0.3	572.68	-10.6	-10.53	-0.08
2	-8.33	-0.3	77.45	-10.42	-10.24	-0.19
3	-7.56	-0.27	2.87	-9.65	-9.51	-0.14
4	-6.85	-0.24	9.50	-8.94	-8.84	-0.1
5	-6.58	-0.24	15.11	-8.66	-8.64	-0.02
6	-6.42	-0.23	19.75	-8.51	-8.38	-0.13
7	-6.33	-0.23	22.89	-8.42	-8.37	-0.05
8	-5.92	-0.21	45.96	-8.01	-7.81	-0.19
9	-4.51	-0.16	491.66	-6.6	-6.57	-0.03

Table 4. Docking results of chalcone derivative **3** into MMP-9 (PDB: 1GKC) catalytic domain. Binding, Intermolecular, VdW, and Electrostatic Energy are reported in kcal/mol; Ligand Efficiency is in kcal/mol/atom; and the Inhibition Constant is in nM.

Pose	Binding Energy (Kcal/mol)	Ligand Efficiency (Kcal/mol/atom)	Inhibition Constant (nM)	Intermolecular Energy (Kcal/mol)	Vdw Energy (Kcal/mol)	Electrostatic Energy (Kcal/mol)
1	-11.92	-0.43	1.82	-14.01	-13.63	-0.38
2	-11.6	-0.41	3.15	-13.69	-13.19	-0.49
3	-10.18	-0.36	34.77	-12.26	-11.87	-0.4
4	-9.65	-0.34	83.95	-11.74	-11.42	-0.32
5	-9.4	-0.34	128.26	-11.49	-11.43	-0.06
6	-8.86	-0.32	321.75	-10.95	-10.77	-0.18
7	-7.96	-0.28	1.45	-10.45	-10.06	-0.97
8	-7.72	-0.28	2.19	-9.81	-9.58	-0.22
9	-7.5	-0.27	3.16	-9.59	-9.39	-0.2

Table 5. Docking results of chalcone derivative **3** into MMP-8 (PDB: 5H8X) catalytic domain. Binding, Intermolecular, VdW, and Electrostatic Energy are reported in kcal/mol; Ligand Efficiency is in kcal/mol/atom; and the Inhibition Constant is in nM.

Pose	Binding Energy (Kcal/mol)	Ligand Efficiency (Kcal/mol/atom)	Inhibition Constant (nM)	Intermolecular Energy (Kcal/mol)	Vdw Energy (Kcal/mol)	Electrostatic Energy (Kcal/mol)
1	-9.90	-0.35	54.99	-11.99	-11.82	-0.17
2	-9.76	-0.35	69.96	-11.85	-11.53	-0.32
3	-7.29	-0.26	4.55	-9.38	-8.93	-0.44
4	-5.83	-0.21	53.54	-7.92	-7.92	0
5	-5.82	-0.21	54.44	-7.91	-7.76	-0.14
6	-5.58	-0.2	81.73	-7.66	-7.34	-0.33
7	-4.62	-0.17	407.62	-6.71	-6.65	-0.06
8	-1.2	-0.04	131.06	-3.29	-3.19	-0.1

Table 6. Docking results of chalcone derivative **3** into MMP-2 (PDB: 8H78) catalytic domain. Binding, Intermolecular, VdW, and Electrostatic Energy are reported in kcal/mol; Ligand Efficiency is in kcal/mol/atom; and the Inhibition Constant is in nM domain.

Pose	Binding Energy (Kcal/mol)	Ligand Efficiency (Kcal/mol/atom)	Inhibition Constant (nM)	Intermolecular Energy (Kcal/mol)	Vdw Energy (Kcal/mol)	Electrostatic Energy (Kcal/mol)
1	-10.45	-0.37	22.02	-12.52	-12.38	-0.16
2	-10.13	-0.36	37.47	-12.22	-11.84	-0.38
3	-8.64	-0.31	464.38	-10.73	-10.63	-0.09
4	-8.43	-0.3	659.45	-10.52	-10.33	-0.19
5	-7.32	-0.26	4.29	-9.41	-9.29	-0.12
6	-6.86	-0.25	9.3	-8.95	-8.8	-0.15
7	-6.36	-0.23	21.76	-8.45	-8.33	-0.12
8	-6.24	-0.22	26.75	-8.33	-8.26	-0.07
9	-5.76	-0.21	59.71	-7.85	-7.74	-0.11

Table 7. Matrix Metalloproteinases alongside their top binding free energies with the docked chalcone derivative **3** calculated through the AD4 docking algorithm, inhibition constants, MMPBSA and key interactions.

Protein	Top Binding Free Energy from AD4 (kcal/mol)	Inhibition Constant (nM)	Binding Affinity (MMPBSA) (Kcal/mol)	Key Interactions
MMP-2	-10.45	22.02	-5.25	Hydrophobic, H-bonds, metal coordination
MMP-8	-9.90	54.99	-5.25	Hydrophobic, H-bonds, ionic
MMP-9	-11.92	1.82	-5.25	Hydrophobic, H-bonds, metal coordination
MMP-10	-8.52	572.68	-5.26	Hydrophobic, H-bonds, ionic
MMP-13	-11.25	5.65	-5.27	Hydrophobic, H-bonds, metal coordination

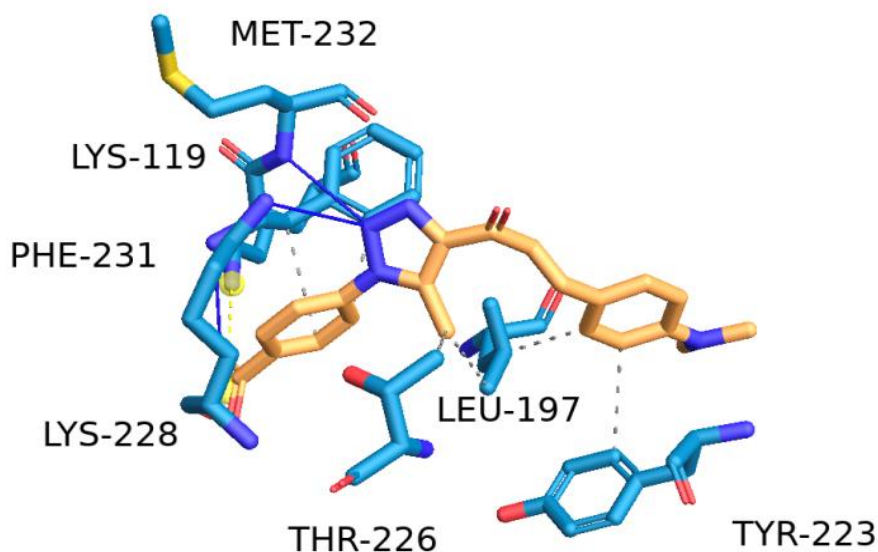


Figure 2. 3D interaction of chalcone derivative within the MMP-13 catalytic domain. Key interactions include hydrophobic interactions (LEU-197, TYR-223), hydrogen bonding (LYS-119, LYS-228, THR-226), and van der Waals contacts (PHE-231, MET-232)..

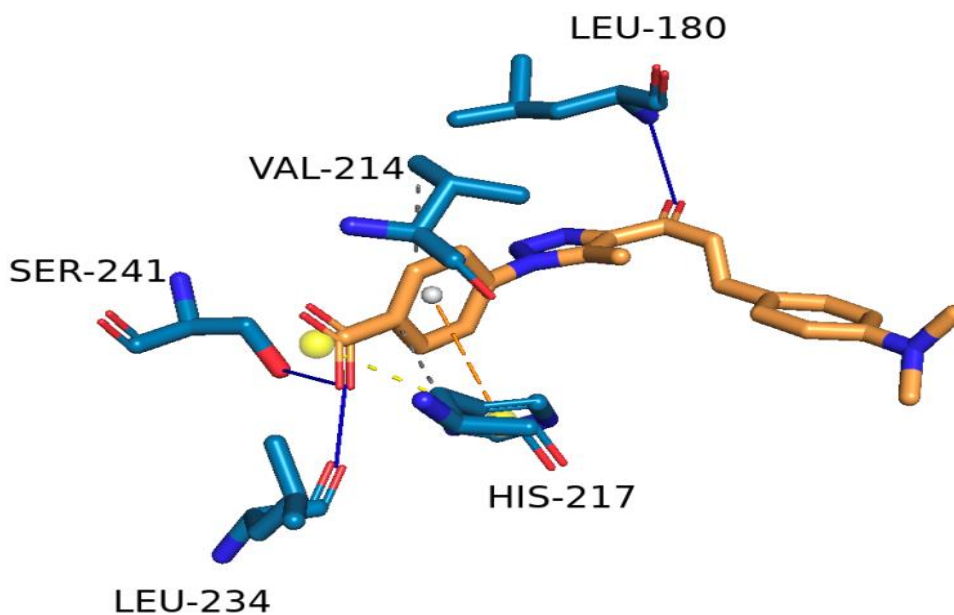


Figure 3. 3D interaction of chalcone derivative within the MMP-10 catalytic domain. Key interactions include hydrogen bonding (HIS-217, SER-241), hydrophobic interactions (LEU-180, VAL-214, LEU-234), and van der Waals contacts stabilizing the complex.

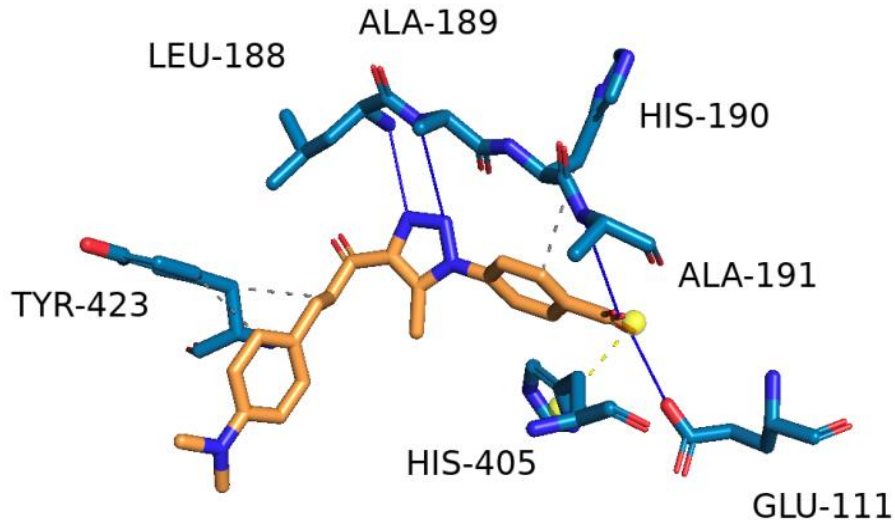


Figure 4. 3D interaction of chalcone derivative within the MMP-9 catalytic domain. Key interactions include hydrogen bonding (HIS-190, ALA-191, GLU-111), hydrophobic interactions (TYR-423, LEU-188, ALA-189), and metal coordination involving HIS-405. These interactions stabilize the compound 3-MMP-9 complex, supporting its strong binding affinity.

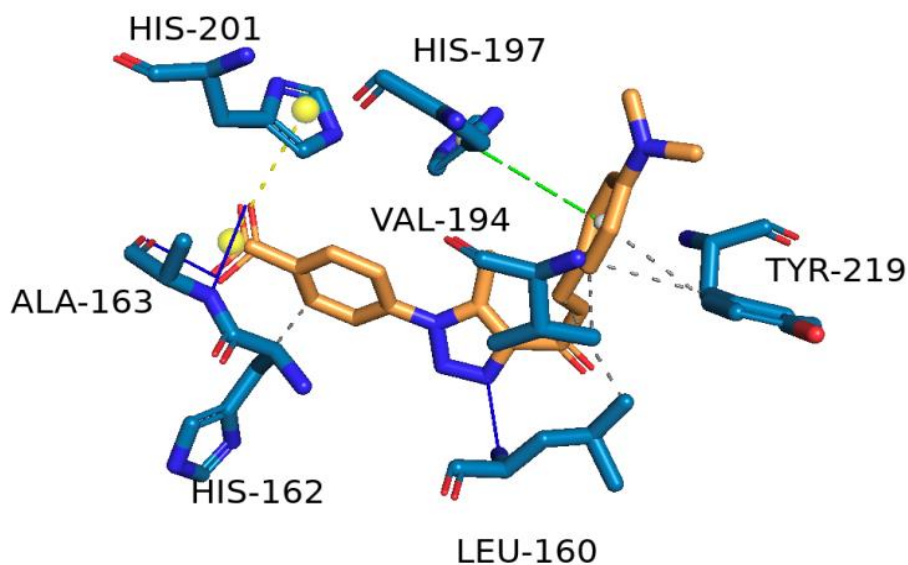


Figure 5. 3D interaction of chalcone derivative within the MMP-8 catalytic domain. Key interactions include hydrogen bonding (HIS-162, ALA-163, HIS-197), hydrophobic interactions (VAL-194, LEU-160, TYR-219), and metal coordination involving HIS-201. These interactions stabilize the compound 3-MMP-8 complex, contributing to its binding profile.

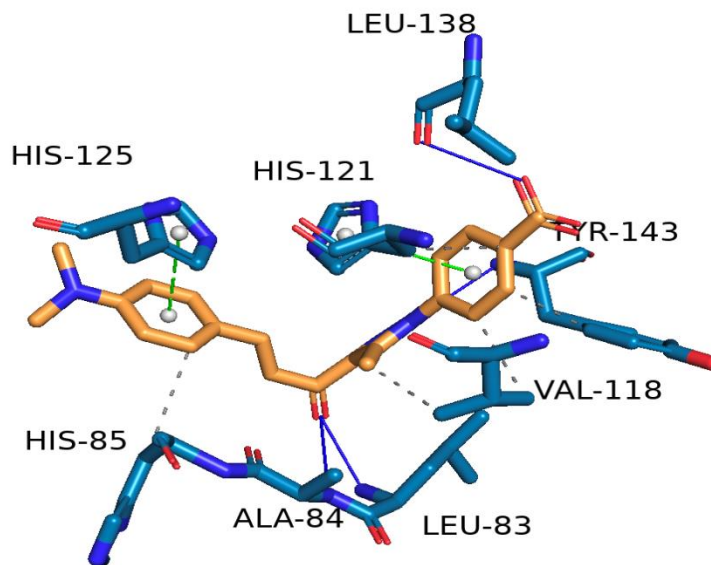


Figure 6. 3D interaction of chalcone derivative within the MMP-2 catalytic domain. Key interactions include hydrogen bonding (HIS-85, HIS-121, ALA-84), hydrophobic interactions (LEU-83, VAL-118, LEU-138), and coordination with HIS-125. These interactions contribute to the stabilization of the compound 3-MMP-2 complex.

4. Conclusion

This detailed analysis of compound **3** binding to MMPs family proteins underscores its preferential inhibition of MMP-9 and MMP-13. The favorable binding energies, low inhibition constants, and strong electrostatic and vdW interactions position compound **3** as a promising candidate for targeted MMPs inhibition. Further experimental validation is warranted to confirm its therapeutic potential.

5. Experimental

5.1. Chemistry

Synthesis of (E)-4-(4-(3-(4-(dimethylamino)phenyl)acryloyl)-5-methyl-1H-1,2,3-triazol-1-yl)benzoic acid 3

To a solution of 4-(4-acetyl-5-methyl-1H-1,2,3-triazol-1-yl)benzoic acid (0.4 g, 1.6 mmol) **1** in ethanol (20 mL) potassium hydroxide (0.27 g, 4.8 mmol) solution in the less amount of water was added. The reaction mixture was stirred for 10 min at room temperature. Then 4-(dimethylamino)benzaldehyde **2** (1.6 mmol) was added. The reaction mixture was stirred for 72 h at room temperature. Excess amount of KOH dissolved in the minimal amount of water was added during the reaction period until the reaction was complete. The reaction mixture was kept in an ice bath while adding KOH to prevent overheating. After completion of the reaction, the reaction mixture was neutralized by iced 1N HCl. The product was then filtered, washed with water, and recrystallized from methanol afforded the pure product [45].

The prepared compound **3** was obtained as orange powder, 0.4 g (65%) yield; M.P: 248-250°C; IR (KBr) 3439-2556 (br, OH), 1720 (C=O carboxylic acid), 1604 (C=O chalcone) cm^{-1} ; ^1H -

NMR (500 MHz: $\text{DMSO-}d_6$): δ 2.60 (s, 3H, CH_3), 2.97 (s, 6H, 2 CH_3), 6.71 (d, $J = 9$ Hz, 2H, 2Ar-H), 7.60 (d, $J = 8.95$ Hz, 2H, 2Ar-H), 7.69-7.80 (m, 4H, 2Ar-H+ $\text{CH}=\text{CH}-\text{CO}$), 8.14 (d, $J = 8.5$ Hz, 2H, 2Ar-H), 13.39 (br. s, H, COOH). ^{13}C -NMR (125 MHz: $\text{DMSO-}d_6$): δ 10.53, 39.50, 40.50 (SP^3 CH), 112.41, 117.31, 122.12, 125.98, 131.22, 132.58, 138.94, 144.10, 144.82, 152.65 (SP^2 Ar-C, SP^2 $\text{CH}=\text{CH}-\text{CO}$), 166.94 (COOH), 183.52 ($\text{CH}=\text{CH}-\text{CO}$). Elemental analysis Calculated for Molecular formula $\text{C}_{21}\text{H}_{20}\text{N}_4\text{O}_3$: C, 67.01; H, 5.36; N, 14.88. Found: C, 67.56; H, 5.78; N, 14.03.

5.2. Docking simulations

The chalcone derivative **3** was drawn using ChemDraw Software (Revvity Signals Software) and converted into three-dimensional structures using Avogadro software [46], adding hydrogen atoms and optimising geometry using the MMFF94 force field. Energy minimisation was carried out to ensure stable conformations of the ligand. Additionally, Gasteiger charges were assigned to facilitate docking calculations using the AutoDockTools (ADT) ligand preparation module [47,48]. The protein structure of MMP-13, MMP-10, MMP-9, MMP-8, and MMP-2 were retrieved from the Protein Data Bank (PDB IDs: 2OW9, 1Q3A, 1GKC, 5H8X, and 8H78, respectively) and used as the docking target. Protein preparation was conducted using AutoDockTools (ADT) 4.2, wherein all unwanted solvents and water molecules were removed from the structure. Polar hydrogens were added to the protein, and Kollman charges were assigned to ensure proper electrostatic interactions. To identify the potential binding site of the MMPs array of targets, the interaction of the co-crystallized ligands present in their respective PDB structure was analysed closely using the

Protein-Ligand Interaction Profiler (PLIP) [43]. Based on the identified binding pocket specifications (Table 1), the grid size was set to $40 \times 40 \times 40$ points with a spacing of 0.375 Å between grid points. The GPF included receptor and ligand atom types to generate atom-specific maps for the different atom types, including electrostatic potential maps and desolvation maps for docking. Docking simulations were performed using AutoDock 4.2 [47,48]. The docking parameter file (DPF) was configured with the genetic algorithm (GA) for flexible ligand docking. The GA settings included a population size of 150, a maximum of 25 million energy evaluations, and up to 27,000 generations. The mutation rate was set to 0.02, while the crossover rate was 0.8. Local search parameters were optimised using the Solis & Wets algorithm, with 300 iterations per run. The docking calculations were carried out over 100 GA-LS runs, ensuring diverse sampling of the ligand conformations in the binding pocket. Clustering tolerance was set at 2.0 Å RMSD, and the best-scoring poses were retained for further analysis. Post Docking Analysis was carried out using AutoDock Tools. Interaction was sampled using PLIP [49], binding affinity was calculated using MMPBSA calculation employing PRODIGY webservice [50], finally interaction visualisation was done using The PyMOL Molecular Graphics System, Version 1.2r3pre, Schrödinger, LLC.

Acknowledgement:

The authors thank the Science, Technology & Innovation Funding Authority (STDF), Cairo, Egypt, for funding this work through the Basic Sciences Research Grant (Proposal ID 48085).

References

- [1] Stetler-Stevenson, W. G.; Aznavoorian, S.; Liotta, L. A. Tumor cell interactions with the extracellular matrix during invasion and metastasis. *Annu. Rev. Cell Biol.* 1993, 9, 541–573.
- [2] Walker, C.; Mojares, E.; Del Río Hernández, A. Role of Extracellular Matrix in Development and Cancer Progression. *Int. J. Mol. Sci.* 2018, 19(10), 3028–3058.
- [3] Kessenbrock, K.; Plaks, V.; Werb, Z. Matrix Metalloproteinases: Regulators of the Tumor Microenvironment. *Cell.* 2010, 141(1), 52–67.
- [4] Cathcart, J.; Pulkoski-Gross, A.; Cao, J. Targeting Matrix Metalloproteinases in Cancer: Bringing New Life to Old Ideas. *Genes Dis.* 2015, 2(1), 26–34.
- [5] Curran, S.; Dundas, S. R.; Buxton, J.; Leeman, M. F.; Ramsay, R.; Murray, G. I. Matrix Metalloproteinase/Tissue Inhibitors of Matrix Metalloproteinase Phenotype Identifies Poor Prognosis Colorectal Cancers. *Clinical Cancer Research.* 2004, 10(24), 8229–8234.
- [6] Forget, M.-A.; Desrosiers, R. R.; Béliveau, R. Physiological Roles of Matrix Metalloproteinases: Implications for Tumor Growth and Metastasis. *Can. J. Physiol. Pharmacol.* 1999, 77(7), 465–480.
- [7] Visse, R.; Nagase, H. Matrix Metalloproteinases and Tissue Inhibitors of Metalloproteinases. *Circ. Res.* 2003, 92(8), 827–839.
- [8] Maskos, K. Crystal Structures of MMPs in Complex with Physiological and Pharmacological Inhibitors. *Biochimie.* 2005, 87(3–4), 249–263.
- [9] Schechter, I.; Berger, A. On the Size of the Active Site in Proteases. I. Papain. *Biochem. Biophys. Res. Commun.* 1967, 27(2), 157–162.
- [10] Brown, S.; Meroueh, S.; Fridman, R.; Mobashery, S. Quest for Selectivity in Inhibition of Matrix Metalloproteinases. *Curr. Top. Med. Chem.* 2004, 4(12), 1227–1238.
- [11] Nuti, E.; Tuccinardi, T.; Rossello, A. Matrix Metalloproteinase Inhibitors: New Challenges in the Era of Post Broad-Spectrum Inhibitors. *Curr. Pharmaceut. Des.* 2007, 13, 2087–2100.
- [12] Georgiadis, D.; Yiotakis, A. Specific Targeting of Metzincin Family Members with Small-Molecule Inhibitors: Progress toward a Multifarious Challenge. *Bioorganic and Medicinal Chemistry.* 2008, 16, 8781–8794.
- [13] Rao, B. G. Recent Developments in the Design of Specific Matrix Metalloproteinase Inhibitors Aided by Structural and Computational Studies. *Curr. Pharmaceut. Des.* 2005, 11, 295–322.
- [14] Coussens, L. M.; Fingleton, B.; Matrisian, L. M. Matrix Metalloproteinase Inhibitors and Cancer—Trials and Tribulations. *Science.* 2002, 295(5564), 2387–2392.
- [15] Breuer, E.; Frant, J.; Reich, R. Recent Non-Hydroxamate Matrix Metalloproteinase Inhibitors. *Expert Opinion on Therapeutic Patents.* 2005, 15, 253–269.
- [16] Whittaker, M.; Floyd, C. D.; Brown, P.; Gearing, A. J. Design and Therapeutic Application of Matrix Metalloproteinase Inhibitors. *Chem. Rev.* 1999, 99(9), 2735–2776.
- [17] Overall, C. M.; Kleifeld, O. Tumour Microenvironment - Opinion: Validating Matrix Metalloproteinases as Drug Targets and Anti-Targets for Cancer Therapy. *Nat. Rev. Cancer.* 2006, 6(3), 227–239.
- [18] Jacobsen, J. A.; Major Jourden, J. L.; Miller, M. T.; Cohen, S. M. To Bind Zinc or Not to Bind Zinc: An Examination of Innovative Approaches to Improved Metalloproteinase Inhibition. *Biochimica et Biophysica Acta (BBA) - Molecular Cell Research.* 2010, 1803, 72–94.
- [19] El Ashry, E. S. H.; Awad, L. F.; Tebeb, M.; Ibrahim, N. A.; Abu-Serie, M. M.; Abd Al Moaty, M. N. Structure-Based Design and Optimization of Pyrimidine- and 1,2,4-Triazolo[4,3-a]Pyrimidine-Based Matrix Metalloproteinase-10/13 Inhibitors via Dimroth Rearrangement towards Targeted Polypharmacology. *Bioorg. Chem.* 2020, 96, 103616.
- [20] Dublanchet, A. C.; Ducrot, P.; Andrianjara, C.; O’Ogara, M.; Morales, R.; Compere, D.; Denis, A.; Blais, S.; Cluzeau, P.; Courté, K. Structure-based Design and Synthesis of Novel Non-Zinc Chelating MMP-12 Inhibitors. *Bioorg. Med. Chem. Lett.* 2005, 15, 3787–3790.

- [21] Li, J. J.; Nahra, J.; Johnson, A. R.; Bunker, A.; O'Brien, P.; Yue, W. S.; Ortwine, D. F.; Man, C. F.; Baragi, V.; Kilgore, K.; Dyer, R. D.; Han, H. K. Quinazolinones and Pyrido[3,4-d]pyrimidin-4-ones as Orally Active and Specific Matrix Metalloproteinase-13 Inhibitors for the Treatment of Osteoarthritis. *J. Med. Chem.* 2008, 51 (3), 835–841.
- [22] Morales, R.; Perrier, S.; Florent, J. M.; Beltra, J.; Dufour, S.; De Mendez, I.; Manceau, P.; Tertre, A.; Moreau, F.; Compere, D. Crystal Structures of Novel Non-Peptidic, Non-Zinc Chelating Inhibitors Bound to MMP-12. *J. Mol. Biol.* 2004, 341 (4), 1063–1076.
- [23] Gamal, H.; Ismail, K. A.; Omar, A. M. M.; Teleb, M.; Abu-Serie, M. M.; Huang, S.; Abdelsattar, A. S.; Zamponi, G. W.; Fahmy, H. Non-Small Cell Lung Cancer Sensitization to Platinum Chemotherapy via New Thiazole-Triazole Hybrids Acting as Dual T-Type CCB/MMP-9 Inhibitors. *J. Enzyme Inhib. Med. Chem.* 2024, 39 (1), 2388209.
- [24] Awad, L. F.; Teleb, M.; Ibrahim, N. A.; Abu-Serie, M. M.; Abd Al Moaty, M. N. Structure-Based Design and Optimization of Pyrimidine- and 1,2,4-Triazolo[4,3-a]Pyrimidine-Based Matrix Metalloproteinase-10/13 Inhibitors via Dimroth Rearrangement towards Targeted Polypharmacology. *Bioorg. Chem.* 2020, 96, 103616.
- [25] Ayoup, M. S.; Fouad, M. A.; Abdel-Hamid, H.; Abu-Serie, M. M.; Noby, A.; Teleb, M. Battle Tactics Against MMP-9: Discovery of Novel Non-Hydroxamate MMP-9 Inhibitors Endowed with PI3K/AKT Signaling Attenuation and Caspase 3/7 Activation via Ugi Bis-Amide Synthesis. *Eur. J. Med. Chem.* 2020, 186, 111875.
- [26] Ayoup, M. S.; Abu-Serie, M. M.; Awad, L. F.; Teleb, M.; Ragab, H. M.; Amer, A. Halting colorectal cancer metastasis via novel dual nanomolar MMP-9/MAO-A quinoxaline-based inhibitors: Design, synthesis, and evaluation. *Eur. J. Med. Chem.* 2021, 222, 113558.
- [27] Haiba, N. S.; Khalil, H. H.; Bergas, A.; Abu-Serie, M. M.; Khattab, S. N.; Teleb, M. First-in-Class Star-Shaped Triazine Dendrimers Endowed with MMP-9 Inhibition and VEGF Suppression Capacity: Design, Synthesis, and Anticancer Evaluation. *ACS Omega* 2022, 7 (24), 21131-21144.
- [28] Khalil, H. H.; Osman, H. A.; Teleb, M.; Darwish, A. I.; Abu-Serie, M. M.; Khattab, S. N.; Haiba, N. S. Engineered s-Triazine-Based Dendrimer-Honokiol Conjugates as Targeted MMP-2/9 Inhibitors for Halting Hepatocellular Carcinoma. *ChemMedChem* 2021, 16(24), 3701-3719.
- [29] Morcos, C. A.; Haiba, N. S.; Bassily, R. W.; Abu-Serie, M. M.; El-Yazbi, A. F.; Soliman, O. A.; Teleb, M. Structure Optimization and Molecular Dynamics Studies of New Tumor-Selective S-Triazines Targeting DNA and MMP-10/13 for Halting Colorectal and Secondary Liver Cancers. *J. Enzyme Inhib. Med. Chem.* 2024, 39 (1), 2423174.
- [30] Khalil, H. H.; El-Sheshtawy, M. M.; Khattab, S. N.; Abu-Serie, M. M.; Shehat, M. G.; Teleb, M.; Haiba, N. S. Chemosensitization of Non-Small Cell Lung Cancer to Sorafenib via Non-Hydroxamate S-Triazinedione-Based MMP-9/10 Inhibitors. *Bioorg. Chem.* 2024, 144, 107155.
- [31] Morcos, C. A.; Khattab, S. N.; Haiba, N. S.; Bassily, R. W.; Abu-Serie, M. M.; Teleb, M. Battling Colorectal Cancer via S-Triazine-Based MMP-10/13 Inhibitors Armed with Electrophilic Warheads for Concomitant Ferroptosis Induction; The First-in-Class Dual-Acting Agents. *Bioorg. Chem.* 2023, 141, 106839.
- [32] Ouyang, Y.; Li, J.; Chen, X.; Fu, X.; Sun, S.; Wu, Q. Chalcone Derivatives: Role in Anticancer Therapy. *Biomolecules* 2021, 11 (6), 894.
- [33] Essa, A. F.; Teleb, M.; El-Kersh, D. M.; El Gendy, A. E. N. G.; Elshamy, A. I.; Farag, M. A. Natural Acylated Flavonoids: Their Chemistry and Biological Merits in Context to Molecular Docking Studies. *Phytochem. Rev.* 2023, 22 (6), 1469-1508.
- [34] El Hawary, S. S.; Khattab, A. R.; Marzouk, H. S.; El Senousy, A. S.; Alex, M. G.; Aly, O. M.; Teleb, M.; Abdelmohsen, U. R. In Silico Identification of SARS-CoV-2 Spike (S) Protein–ACE2 Complex Inhibitors from Eight Tecoma Species and Cultivars Analyzed by LC-MS. *RSC Adv.* 2020, 10 (70), 43103-43108.
- [35] Khattab, A. R.; Teleb, M.; Kamel, M. S. In Silico Study of Potential Anti-SARS Cell Entry Phytoligands from *Phlomis aurea*: A Promising Avenue for Prophylaxis. *Future Virology* 2021, 16 (11), 761-775.
- [36] Khattab, A. R.; Teleb, M. In Silico Discovery of Non-Psychoactive Scaffolds in Cannabis Halting SARS-CoV-2 Host Entry and Replication Machinery. *Future Virology* 2022, 17 (6), 367-386.
- [37] Spahn, V.; Del Vecchio, G.; Labuz, D.; Rodriguez-Gaztelumendi, A.; Massaly, N.; Temp, J.; Durmaz, V.; Sabri, P.; Reidelbach, M.; Machelska, H.; Weber, M.; Stein, C. A Nontoxic Pain Killer Designed by Modeling of Pathological Receptor Conformations. *Science* 2017, 355 (6328), 966–969.
- [38] Udier-Blagović, M.; Tirado-Rives, J.; Jorgensen, W. L. Validation of a Model for the Complex of HIV-1 Reverse Transcriptase with Nonnucleoside Inhibitor TMC125. *J. Am. Chem. Soc.* 2003, 125 (20), 6016–6017.
- [39] Hou, T.; Wang, J.; Li, Y.; Wang, W. Assessing the Performance of the MM/PBSA and MM/GBSA Methods. 1. The Accuracy of Binding Free Energy Calculations Based on Molecular Dynamics Simulations. *J. Chem. Inf. Model.* 2011, 51 (1), 69–82.
- [40] Johnson, A. R.; Pavlovsky, A. G.; Ortwine, D. F.; Prior, F.; Man, C. F.; Bornemeier, D. A.; Banotai, C. A.; Mueller, W. T.; McConnell, P.; Yan, C.; Baragi, V. Discovery and Characterization of a Novel Inhibitor of Matrix Metalloprotease-13 That Reduces Cartilage Damage In Vivo without Joint Fibroplasia Side Effects. *J. Biol. Chem.* 2007, 282 (38), 27781–27791.
- [41] Bertini, I.; Calderone, V.; Fragai, M.; Luchinat, C.; Mangani, S.; Terni, B. Crystal Structure of the Catalytic Domain of Human Matrix Metalloproteinase 10. *J. Mol. Biol.* 2004, 336 (3), 707-716.

- [42] Rowsell, S.; Hawtin, P.; Minshull, C. A.; Jepson, H.; Brockbank, S. M.; Barratt, D. G.; Slater, A. M.; McPheat, W. L.; Waterson, D.; Henney, A. M.; Paupit, R. A. Crystal Structure of Human MMP9 in Complex with a Reverse Hydroxamate Inhibitor. *J. Mol. Biol.* 2002, 319 (1), 173-181.
- [43] Tauro, M.; Laghezza, A.; Loiodice, F.; Piemontese, L.; Caradonna, A.; Capelli, D.; Montanari, R.; Pochetti, G.; Di Pizio, A.; Agamennone, M.; Campestre, C. Catechol-Based Matrix Metalloproteinase Inhibitors with Additional Antioxidative Activity. *J. Enzyme Inhib. Med. Chem.* 2016, 31 (suppl 4), 25-37.
- [44] Takeuchi, T.; Nomura, Y.; Tamita, T.; Nishikawa, R.; Kakinuma, H.; Kojima, N.; Hitaka, K.; Tamura, Y.; Kamitani, M.; Mima, M.; Nozoe, A. Discovery of TP0597850: A Selective, Chemically Stable, and Slow Tight-Binding Matrix Metalloproteinase-2 Inhibitor with a Phenylbenzamide-Pentapeptide Hybrid Scaffold. *J. Med. Chem.* 2023, 66(1), 822-836.
- [45] El-Wakil, M. H.; Khattab, S. N.; El-Yazbi, A. F.; El-Nikhely, N.; Soffar, A.; Khalil, H. H. New Chalcone-Tethered 1,3,5-Triazines Potentiate the Anticancer Effect of Cisplatin Against Human Lung Adenocarcinoma A549 Cells by Enhancing DNA Damage and Cell Apoptosis. *Bioorg. Chem.* 2020, 105, 104393.
- [46] Hanwell, M. D.; Curtis, D. E.; Lonie, D. C.; Vandermeersch, T.; Zurek, E.; Hutchison, G. R. Avogadro: An Advanced Semantic Chemical Editor, Visualization, and Analysis Platform. *J. Cheminformatics* 2012, 4, 1-17.
- [47] Forli, S.; Huey, R.; Pique, M. E.; Sanner, M. F.; Goodsell, D. S.; Olson, A. J. Computational Protein-Ligand Docking and Virtual Drug Screening with the AutoDock Suite. *Nat. Protoc.* 2016, 11 (5), 905-919.
- [48] Huey, R.; Morris, G. M.; Olson, A. J.; Goodsell, D. S. A Semiempirical Free Energy Force Field with Charge-Based Desolvation. *J. Comput. Chem.* 2007, 28 (6), 1145-1152.
- [49] Adasme, M. F.; Linnemann, K. L.; Bolz, S. N.; Kaiser, F.; Salentin, S.; Haupt, V. J.; Schroeder, M. PLIP 2021: Expanding the Scope of the Protein-Ligand Interaction Profiler to DNA and RNA. *Nucleic Acids Res.* 2021, 49 (W1), W530-W534.
- [50] Xue, L. C.; Rodrigues, J. P.; Kastritis, P. L.; Bonvin, A. M.; Vangone, A. PRODIGY: A Web Server for Predicting the Binding Affinity of Protein-Protein Complexes. *Bioinformatics* 2016, 32 (23), 3676-3678.